Nonlinear Dyn (2022) 107:855–870
https://doi.org/10.1007/s11071-021-07054-2

ORIGINAL PAPER

Feature extraction based on generalized permutation entropy for condition monitoring of rotating machinery

Jinshan Lin · Chunhong Dou · Yingjie Liu

Received: 2 July 2021 / Accepted: 6 November 2021 / Published online: 22 November 2021

Abstract Defective rotating machinery usually exhibits complex dynamic behavior. Therefore, feature representation of machinery vibration signals is always critical for condition monitoring of rotating machinery. Permutation entropy (PeEn), an adaptive symbolic description, can measure complexities of signals. However, PeEn, which compresses all the information into a single parameter, may lack the capability to fully describe the dynamics of complex signals. Afterward, multiscale PeEn (MPeEn) is put forward for coping with nonstationarity, outliers and artifacts emerging in complex signals. In MPeEn, a set of parameters serves to describe the dynamics of complex signals in different time scales. Nonetheless, an average procedure in MPeEn may withhold local information of complex signals and destroy internal structures of complex signals. To overcome deficiencies of PeEn and MPeEn, this paper proposes generalized PeEn (GPeEn) by introducing different orders and time lags into PeEn. In GPeEn, a complex signal is converted into a PeEn matrix rather than a single parameter. Moreover, minimal, maximal and average values of the PeEn matrix serve to briefly describe conditions of rotating machinery. Next, a numerical experiment proves that the proposed method in this paper performs better than skewness, kurtosis, PeEn and MPeEn in characterizing conditions of a Lorenz model. Subsequently, the proposed method in this paper is compared with skewness, kurtosis, PeEn and MPeEn by investigating gear and roll-bearing vibration signals containing different types and severity of faults. The results show that the proposed method in this paper outperforms the other four methods in distinguishing between different types and severity of faults of rotating machinery.

Keywords Feature extraction · Permutation entropy · Multiscale permutation entropy · Generalized permutation entropy · Condition monitoring · Rotating machinery

J. Lin (✉) · Y. Liu
School of Mechatronics and Vehicle Engineering, Weifang University, Weifang 261061, China
e-mail: jslinmec@hotmail.com; jslinmec@wfu.edu.cn

C. Dou
School of Information and Control Engineering, Weifang University, Weifang 261061, China

1 Introduction

Defective rotating machinery usually displays complex nonstationarity and nonlinearity [1–4]. As a result, feature representation of machinery vibration signals is always a central problem for condition monitoring of rotating machinery [2, 3, 5]. Currently, some methods for time–frequency analysis, such as wavelet transform (WT) and empirical mode decomposition (EMD), have been exploited for feature

extraction of machinery vibration signals [6–9]. However, either of WT and EMD seemingly encounters some difficulties in analyzing complex machinery vibration signals [10–13]. A lot of references have indicated that vibration signals from defective rotating machinery display obvious fractal and chaotic properties [1, 14–18]. Consequently, extraction of nonlinear features from vibration signals is critically important for gaining an insight into the dynamics of machinery. Then, phase space reconstruction (PSR) has been adopted to reveal nature of complex machinery vibration signals [19, 20]. Nevertheless, it seems difficult for PSR to determine two important parameters, i.e., the embedding dimension and the time lag [21]. Next, multifractal detrended fluctuation analysis (MFDFA) was applied to examine the dynamics of complex machinery vibration signals [1, 15, 17, 18]. Nonetheless, MFDFA needs refining further since suffering from some shortages [1, 18]. Hence, nonlinear feature extraction for condition monitoring of rotating machinery leaves much to be desired [22].

Symbolic dynamics, a coarse-graining or description-reduction method, can remain chaotic properties of complex signals but discards considerable details [23]. Therefore, a symbolic description is effective for demonstrating nature of complex signals [14, 16]. Currently, symbolic dynamics has been employed to capture essence of machinery vibration signals [14, 16]. Traditionally, a symbolic description can convert an original signal into several symbols in terms of a preset threshold [23]. As a result, the threshold-based symbolic method is rather short of adaptation. Next, permutation entropy (PeEn), an adaptive symbolic description, was proposed for measuring complexities of signals [24]. With presetting a permutation order and a time lag, PeEn can adaptively transform an original signal into a set of symbols by comparing neighboring values of the signal. Currently, PeEn has found its application in various research fields [25–28]. However, PeEn, which compresses all the information into a single parameter, may lack the capability to fully describe the dynamics of complex signals [24]. Afterward, PeEn based on non-uniform embedding was presented for dealing with time series with non-uniform embedding [29]. Nevertheless, it seems difficult to select an optimal set of time lags. Moreover, Ref. [30] investigated impacts of equalities in an input signal on results of PeEn. Additionally, a generalized PeEn was presented for applying PeEn to random processes [31]. Also, multiscale PeEn (MPeEn) was put forward for coping with nonstationarity, outliers and artifacts emerging in complex signals [32, 33]. In MPeEn, a set of parameters serves to describe the dynamics of complex signals in different time scales. Notwithstanding, an average procedure in MPeEn may withhold local information of complex signals and destroy internal structures of complex signals. In fact, a complex dynamic system may display different dynamic behavior in different permutation orders and time lags [34]. To relieve shortages of PeEn and MPeEn, this paper broads the definition of PeEn by introducing different orders and time lags into PeEn. Thus, this paper proposes another generalized PeEn (GPeEn) for characterizing dynamics of complex signals. Here, it must be noticed that the concept of GPeEn proposed in this paper is distinctly different from that proposed in Ref. [31]. In GPeEn, a complex signal is converted into a PeEn matrix rather than a single parameter. Moreover, minimal, maximal and average values of the PeEn matrix serve to briefly describe conditions of rotating machinery. Next, the performance of the proposed method in this paper was benchmarked against that of skewness, kurtosis, PeEn and MPeEn by analyzing time series generated in a Lorenz model. In addition, the proposed method in this paper was compared with skewness, kurtosis, PeEn and MPeEn by investigating gear and rolling-bearing vibration signal containing different types and severity of faults. The results show that the proposed method in this paper is clearly superior to skewness, kurtosis, PeEn and MPeEn in condition monitoring of rotating machinery.

This paper is structured as follows. Section 2 formulates PeEn and MPeEn, proposes GPeEn and develops a novel method for feature extraction based on GPeEn. In Sect. 3, the performance of the proposed method in this paper is benchmarked numerically against that of skewness, kurtosis, PeEn and MPeEn by examining a Lorenz model. In Sect. 4, the proposed method in this paper is compared experimentally with skewness, kurtosis, PeEn and MPeEn by investigating gear and bearing vibration signals containing different types and severity of faults. Finally, Sect. 5 concludes this paper.

2 Generalized permutation entropy (GPeEn)

2.1 PeEn

The theoretical basis of PeEn was formed in Ref. [24, 35, 36]. Furthermore, a time series $x_t(t = 1, 2, \ldots, T)$, where T indicates the length of the series x_t, can be converted into an m-order embedding phase space with time lag l as follows [37].

$$X_i = \{x_i, x_{i+l}, \ldots, x_{i+(m-1)l}\}, \quad 1 \le i \le T - (m-1)l \tag{1}$$

Here, m and l represent the embedding order and the time lag, respectively. For an arbitrary i, the m number of real values X_i is arranged in an ascending order as follows.

$$\left[x_{i+(j_1-1)l} \le x_{i+(j_2-1)l} \le \cdots \le x_{i+(j_m-1)l}\right] \tag{2}$$

When two successive elements in X_i are equal, for example, $x_{i+(j_1-1)l} = x_{i+(j_2-1)l}$, one can record $x_{i+(j_1-1)l} \le x_{i+(j_2-1)l}$ if $j_1 < j_2$. As a result, any vector X_i can be uniquely projected to $(j_1, j_2, \ldots, j_m)$. This means that a point corresponding to the vector X_i in the m-order embedding phase space can be represented by symbols. For this reason, the m-order embedding phase space can be described by a symbol series.

For x_t, there are at most $m!$ permutations for order m. The relative frequency $p(\psi)$ for each permutation ψ is given as follows.

$$p(\psi) = \frac{F\{t | t \le T - m, (x_{t+1}, \ldots, x_{t+m}) \text{ has type } \psi\}}{T - m + 1} \tag{3}$$

Here, ψ represents a permutation type, $F(\psi)$ refers to the absolute number of occurrences of ψ and $p(\psi)$ indicates the relative frequency of occurrences of ψ.

The permutation entropy h_m for order $m \ge 2$ is defined as follows.

$$h_m = -\sum p(\psi) \log[p(\psi)] \tag{4}$$

As shown in Eq. (4), for a specific order and a specific time lag, PeEn can compress all the information of a time series into a single parameter. When the investigated time series is completely random, which means the relative frequency $p(\psi)$ for each permutation ψ is uniform, i.e., $p(\psi) = 1/m!$, the PeEn h_m achieves the maximum value $h_p = \ln(m!)$. In some cases, the PeEn h_m is normalized by $\ln(m!)$ as follows [36].

$$0 \le h_m / \ln(m!) \le h_p / \ln(m!) = 1 \tag{5}$$

Moreover, when the investigated time series is completely deterministic, the PeEn h_m achieves the minimum value. Thus, the PeEn h_m can serve to demonstrate properties of a time series: The larger the PeEn h_m is, the more random the investigated time series is. Accordingly, the maximum and the minimum values of the PeEn h_m relate to the nature of a time series.

2.2 MPeEn

MPeEn introduces a multiscale concept to PeEn. For a time series $x_t(t = 1, 2, \ldots, T)$, where T indicates the length of the series x_t, a calculation procedure of MPeEn includes the following three steps.

(1) Convert the original series x_t into a coarse-graining one as follows.

$$y_j^\tau = \frac{1}{\tau} \sum_{i=(j-1)\tau+1}^{j\tau} x_i, \quad 1 \le j \le N_\tau = \text{int}\left(\frac{T}{\tau}\right) \tag{6}$$

Here, τ stands for a scale factor and the sign $\text{int}(\cdot)$ means to round down a figure. Thus, the original series x_t is divided into N_τ non-overlapping data windows with the same size τ. Consequently, a coarse-graining series $y_j^\tau (j = 1, 2, \ldots, N_\tau)$ is generated.

(2) Calculate the PeEn h_m^τ of the coarse-graining series $y_j^\tau (i = 1, 2, \ldots, N_\tau)$.

(3) Change the window size $\tau(\tau = \tau_1, \tau_2, \ldots, \tau_s)$, where τ_j and s represent the jth window size and the window number, respectively, repeat the above two steps and finally obtain MPeEn, i.e., a sequence of $h_m^\tau(\tau = \tau_1, \tau_2, \ldots, \tau_s)$.

2.3 Feature extraction based on GPeEn

In GPeEn, different orders and time lags are considered for a time series $x_t(t = 1, 2, \ldots, T)$. Here, GPeEn has the lag number L and the order number N. Also, $\psi_{l,m}$ represents a permutation with lag $l(1 \le l \le L)$ and

order $m(1 \le m \le N)$. As such, the relative frequency $p(\psi_{l,m})$ for each permutation $\psi_{l,m}$ is given as follows.

$$p(\psi_{l,m}) = \frac{F\{t|t \le T - ml, (x_{t+l}, x_{t+2l}, \ldots, x_{t+ml}) \text{ has type } \psi_{l,m}\}}{T - ml + 1} \tag{7}$$

The GPeEn $h_{l,m}$ for order $m \ge 2$ is defined as follows.

$$h_{l,m} = -\sum p(\psi_{l,m}) \log[p(\psi_{l,m})] \tag{8}$$

Considering different orders and time lags for GPeEn, one can convert a time series to a PeEn matrix whose size is $L \times N$. Obviously, the PeEn matrix obtained by GPeEn contains more information than a single parameter done by PeEn.

When the investigated time series in some order and time lag is completely random, which means the relative frequency $p(\psi_{l,m})$ for each permutation $\psi_{l,m}$ is uniform, i.e., $p(\psi_{l,m}) = 1/(L \times N)! = 1/P!$, where $P = L \times N$, the GPeEn $h_{l,m}$ achieves the maximum value $h_{Gp} = \ln(P!)$. In some cases, the GPeEn $h_{l,m}$ is also normalized by $\ln(P!)$ as follows.

$$0 \le h_{l,m}/\ln(P!) \le h_{Gp}/\ln(P!) = 1 \tag{9}$$

Moreover, when the investigated time series in some time lag and some order is completely deterministic, the GPeEn $h_{l,m}$ achieves the minimum value. Furthermore, an average value of the GPeEn $h_{l,m}$ can be used to describe collective properties of the PeEn matrix. Accordingly, the minimum, the maximum and the average values of the PeEn matrix have the capability to release essential details of a time series.

The PeEn matrix with the size $L \times N$ seems rather redundant in describing properties of complex signals. Afterward, this paper exploits the minimal, the maximal and the average values of the PeEn matrix to briefly describe the dynamics of complex signals. Consequently, this paper proposes a novel method for feature extraction based on GPeEn.

3 Application of GPeEn to Lorenz chaotic series

The feasibility of the proposed method in this paper was evaluated by examining a time series generated in a Lorenz model, which is formulized as follows.

$$\begin{cases} \dot{x} = \sigma(y - x) \\ \dot{y} = rx - y - xz \\ \dot{z} = xy - bz \end{cases} \tag{10}$$

In the Lorenz model, $\sigma = 10$ and $b = 8/3$. As known well, the Lorenz model demonstrates different dynamics for different Rayleigh numbers r. When $0 < r < 13.9656$, the Lorenz model does not relate to chaos. When $13.9656 < r < 24.06$, the Lorenz model relates to transient chaos. When $r > 24.06$, the Lorenz model relates to chaos. Finer details on the Lorenz model can refer to Ref. [38]. In this paper, r is assigned one value at a time from [0.7 1.2 10 19 21 24.5 30 40]. Then, the Lorenz model is solved using the 4-order Runge–Kutta algorithm, with the initial point $[x_0 \quad y_0 \quad z_0] = [0 \quad 1 \quad 1.05]$, the time interval $T = [0 \quad 10^5]$ and the ode solver precision 10^{-6}. First, the skewness of the solutions of x for different r was calculated, and the results are illustrated in Fig. 1. As illustrated in Fig. 1, the skewness of the solutions of x for r = 0.7, 1.2 and 10, which corresponds to non-chaos, has a considerable fluctuation. Also, skewness, identical for r = 24.5, 30 and 40, fails to distinguish between these conditions. In what follows, the kurtosis of the solutions of x for different r was calculated and the results are illustrated in Fig. 2. As illustrated in Fig. 2, the kurtosis of the solutions of x for r = 0.7, 1.2 and 10, which corresponds to non-chaos, has a considerable fluctuation. Additionally, kurtosis, identical for r = 24.5, 30 and 40, is unsuccessful in distinguishing between these conditions. Next, PeEn was applied to examine the solutions of x for different r, and the results are demonstrated in Fig. 3. As demonstrated in Fig. 3, PeEn remains constant for r = 0.7, 1.2 and 10 and does the same for r = 24.5, 30 and 40. Although successful in distinguishing between non-chaos, transient chaos and chaos, PeEn fails to distinguish between conditions for r = 0.7, 1.2 and between those for r = 24.5, 30 and 40. In the following, MPeEn was employed to decode the solutions of x for different r and the results are demonstrated in Fig. 4. In this paper, time scales in MPeEn are set as $[1, 2, \ldots, 20]$. As demonstrated in Fig. 4, although capable of distinguishing chaos from the other conditions, MPeEn cannot serve to distinguish between non-chaos and transient chaos. Next, GPeEn was employed to analyze the solutions of x for different r, and the color maps of the PeEn matrix are shown in Fig. 5. In this paper, GPeEn has the time lag

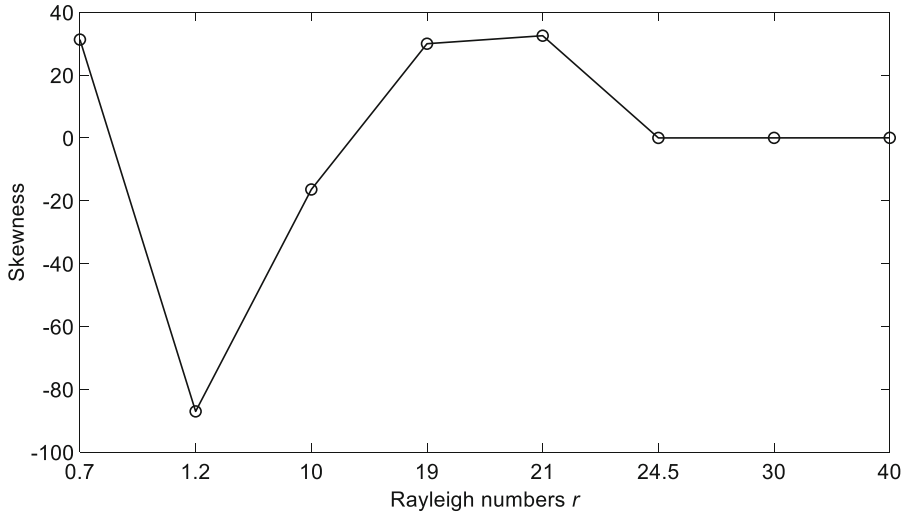

Fig. 1 Skewness of the solutions of x in the Lorenz model for different Rayleigh numbers r

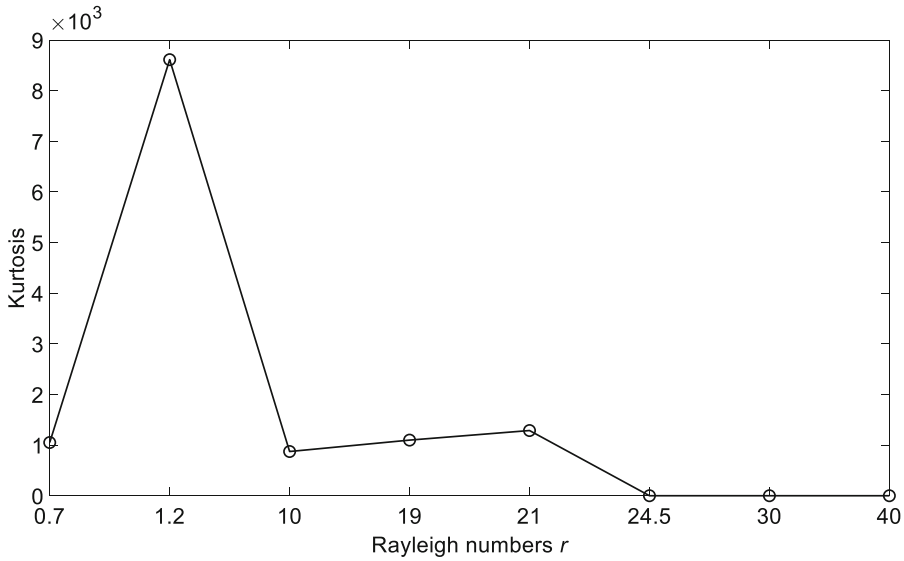

Fig. 2 Kurtosis of the solutions of x in the Lorenz model for different Rayleigh numbers r

range $[1, 2, \ldots, 20]$ and the order range $[3, 4, \ldots, 7]$. As shown in Fig. 5, orders and time lags exert a considerable impact on PeEn. Thus, GPeEn greatly varies with changes of orders and time lags. As a result, the color maps in Fig. 5 can be almost classified as three types: the upper color maps match $0 < r < 13.9656$, which corresponds to non-chaos; the middle color maps match $13.9656 < r < 24.06$, which corresponds to transient chaos; the bottom color maps match $r > 24.06$, which corresponds to chaos. In addition, the color maps for transient chaos produce a sharper fluctuation than those for non-chaos or chaos. For this reason, non-chaos, transient chaos and chaos can be distinguished according to the color maps in Fig. 5. Afterward, the minimum, the maximum and the average values of the PeEn matrix were extracted, and the results are displayed in Fig. 6. As displayed in Fig. 6, these symbols can be clearly divided into three different groups: non-chaos with $0 < r < 13.9656$ in the upper-right corner, transient chaos with $13.9656 < r < 24.06$ in the middle and chaos with $r > 24.06$ in the lower-left corner. This means that the proposed method in this paper can describe conditions of the Lorenz model. In addition, Fig. 6 illustrates that the order and the time lag both in PeEn and in MPeEn are hard to choose since valid for all the conditions.

In general, both PeEn and MPeEn face difficulties in determining optimal orders and time lags. As a

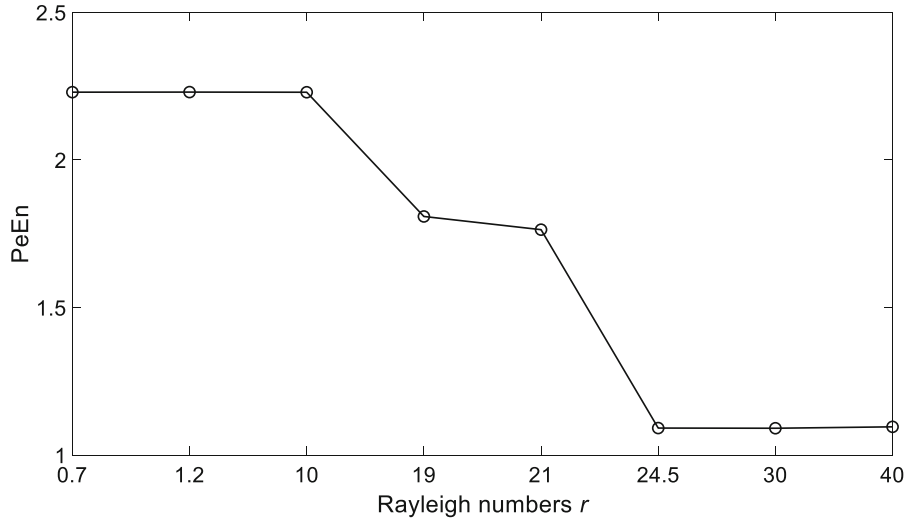

Fig. 3 PeEn of the solutions of x in the Lorenz model for different Rayleigh numbers r

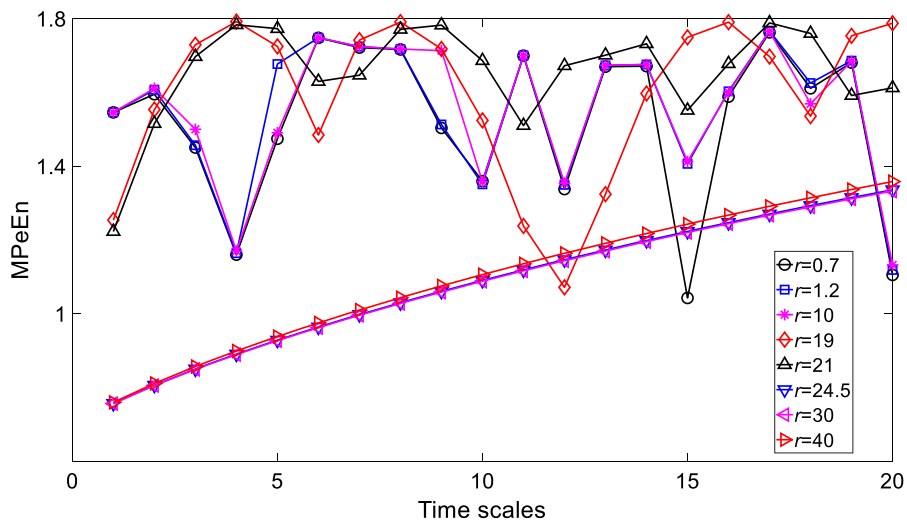

Fig. 4 MPeEn of the solutions of x in the Lorenz model for different time scales

result, both PeEn and MPeEn demonstrate little feasibility for describing an evolving process of a Lorenz model. By contrast, GPeEn, which constructs a PeEn matrix by considering different orders and time lags, performs better in describing dynamics of a Lorenz model.

4 Condition monitoring of rotating machinery

4.1 Condition monitoring of gears

This subsection conducted a gear experiment for modeling gear faults. In the gear experiment described in Fig. 7, a driving motor has a constant speed of 1600 revolutions per minute (RPM). The gear experiment comprises four different types of gear condition: normal, slight-scratch, severe-scratch and broken-tooth. In the gear experiment, sixteen pieces of vibration signals with a sample frequency of 16,384 Hz and a size of 10,000 points were captured from the driving end for each gear condition. These four types of gear vibration signal are demonstrated in Fig. 8.

To begin with, the skewness of these gear vibration signals was estimated and the results are given in Fig. 9. As given in Fig. 9, the skewness for normal and slight-scratch gear conditions overlaps severely. This means that skewness lacks the capability to distinguish between these four types of gear condition. Afterward,

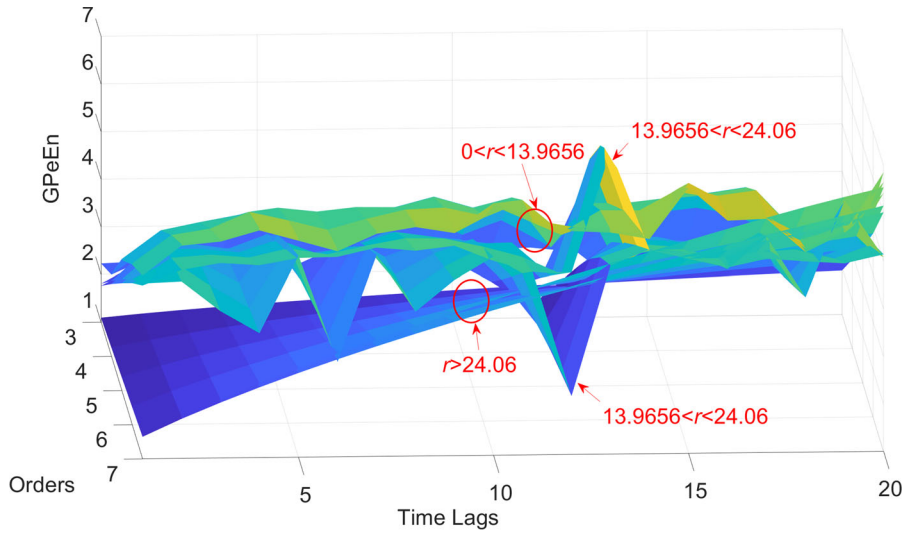

Fig. 5 GPeEn of the solutions of x in the Lorenz model for $r = 0.7,\ 1.2,\ 10,\ 19, 21,\ 24.5,\ 30,\ 40$

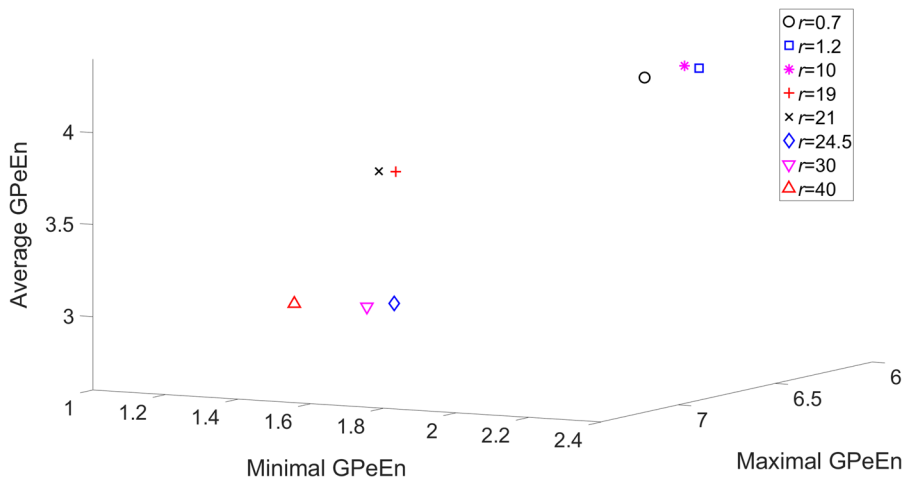

Fig. 6 Minimal, maximal and average values of GPeEn of the solutions of x in the Lorenz model for $r = 0.7,\ 1.2,\ 10,\ 19, 21,\ 24.5,\ 30,\ 40$

the kurtosis of these gear vibration signals was estimated, and the results are given in Fig. 10. Similarly, Fig. 10 indicates that the kurtosis for normal and slight-scratch gear conditions overlaps severely. This proves that kurtosis is scarcely feasible for distinguishing between these four types of gear condition. Next, PeEn was applied to investigate these gear vibration signals, and the results are demonstrated in Fig. 11. As demonstrated in Fig. 11, PeEn can serve to distinguish between these four types of gear condition. However, PeEn for severe-scratch and broken-tooth fluctuates considerably over times. Next, MPeEn was adopted to examine these gear vibration signals, and the results are illustrated in Fig. 12. As illustrated in Fig. 12, MPeEn for these four types of gear condition overlap greatly. In addition, MPeEn for these four types of gear vibration signal fluctuates widely over time scales. Thus, MPeEn seemingly demonstrates little feasibility for discriminating between these four types of gear condition. In the following, GPeEn was made use of analyzing these gear vibration signals. Moreover, minimal, maximal and average values of the PeEn matrix obtained by GPeEn served to distinguish between these four types

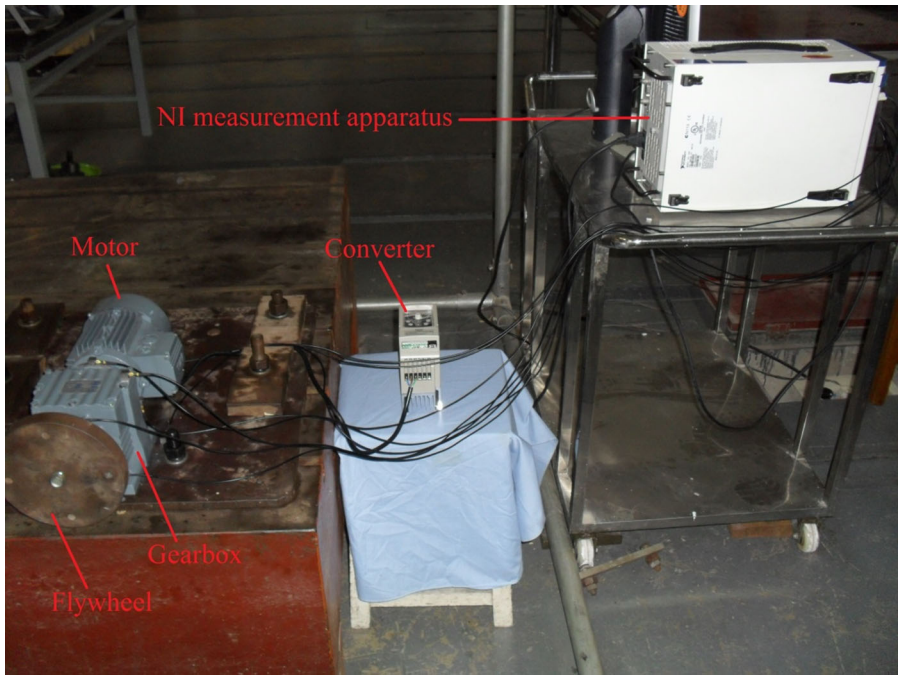

Fig. 7 A gear experiment for modeling gear faults

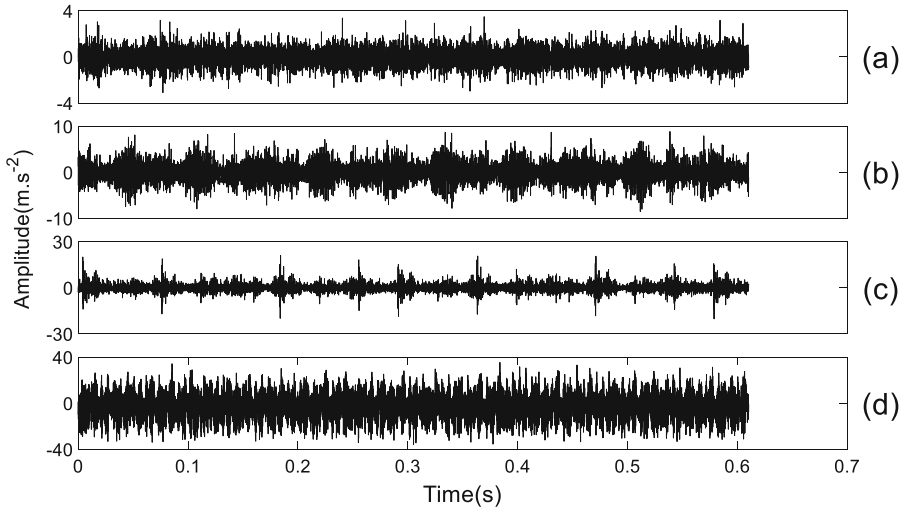

Fig. 8 Four types of gear vibration signal, (a)–(d) for normal, slight-scratch, severe-scratch and broken-tooth, respectively

of gear condition and the results are indicated in Fig. 13. As indicated in Fig. 13, these symbols can be clearly divided into four different groups: normal, slight-scratch, severe-scratch and broken-tooth. Consequently, these four types of gear condition can be clearly separated by the proposed method in this paper.

4.2 Condition monitoring of rolling bearings

This subsection employed rolling-bearing vibration signals from Bearing Data Center of Case Western Reserve University to further measure the performance of the proposed method in this paper. In the bearing experiment described in Fig. 14, the revolving speed of a driving motor fluctuates between 1720 and 1797 RPM. The bearing experiment includes twelve

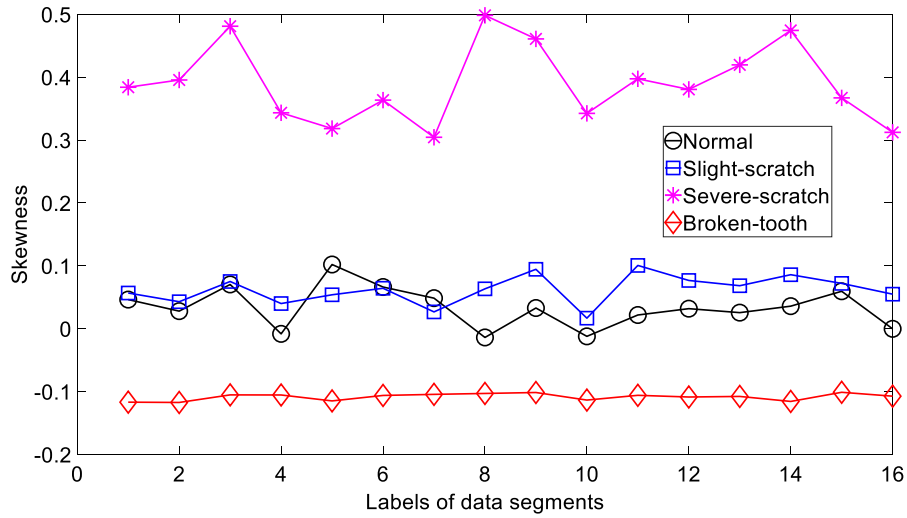

Fig. 9 Skewness for four types of gear vibration signal

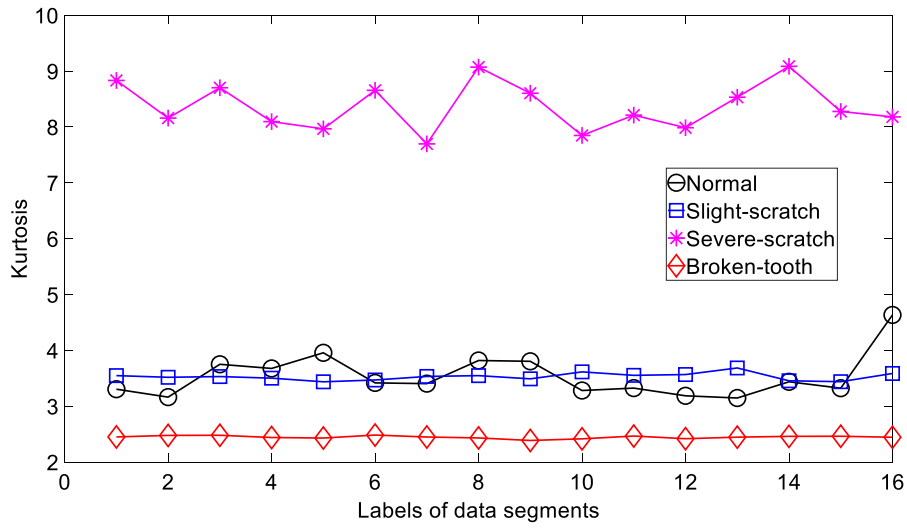

Fig. 10 Kurtosis for four types of gear vibration signal

different types of bearing condition, which are displayed in Table 1. For each bearing condition, six pieces of vibration signals with a sample frequency of 12,000 Hz and a size of 20,000 points were collected from the driving end. These twelve types of bearing vibration signal are displayed in Fig. 15.

To start with, the skewness of these bearing vibration signals was calculated, and the results are demonstrated in Fig. 16. As demonstrated in Fig. 16, the skewness of these bearing vibration signals overlaps severely. This shows that skewness hardly serves to distinguish between these twelve types of bearing condition. In the following, the kurtosis of these bearing vibration signals was calculated, and the results are demonstrated in Fig. 17. Similarly, Fig. 17 illustrates that the kurtosis of these bearing vibration signals overlaps severely. Consequently, this suggests that kurtosis is scarcely feasible for distinguishing between these twelve types of bearing condition. Subsequently, PeEn was utilized to explore these bearing vibration signals, and the results are given in Fig. 18. As given in Fig. 18, except normal, IR028 and OR014, the remaining nine types of bearing condition are hard to separate. After this, MPeEn was used to study these bearing vibration signals, and the results are depicted in Fig. 19. As depicted in Fig. 19, there is considerable overlap between MPeEn of these twelve types of bearing vibration signal. In addition, MPeEn for IR007, IR028 and B014 fluctuates widely over time scales. Furthermore, the proposed method in this

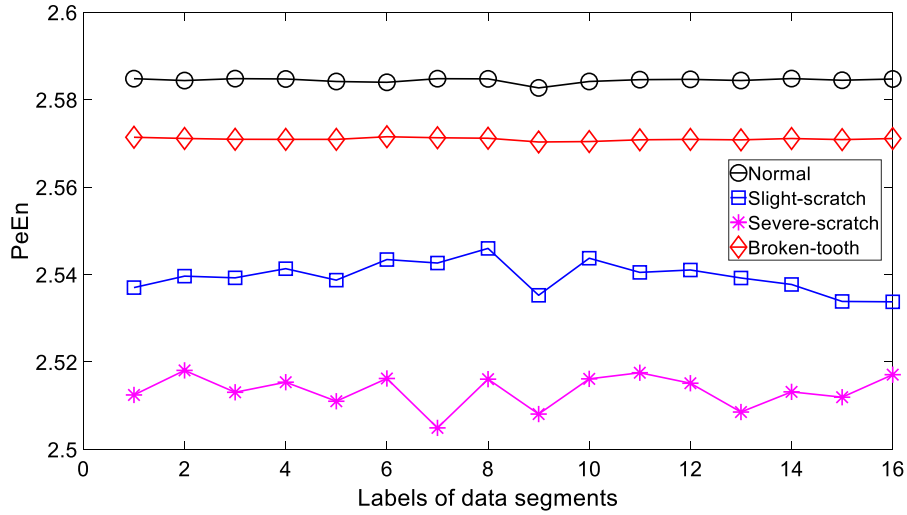

Fig. 11 PeEn for four types of gear vibration signal

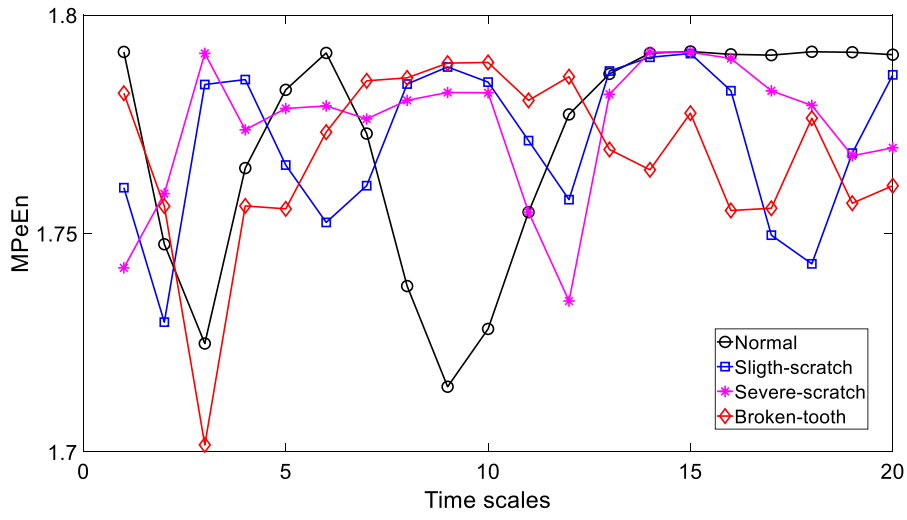

Fig. 12 MPeEn for four types of gear vibration signal

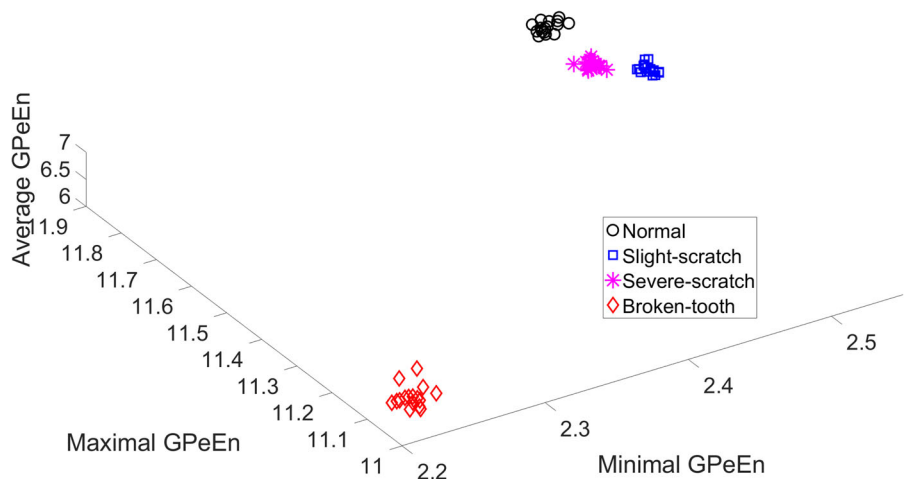

Fig. 13 Separation of four types of gear condition by the proposed method in this paper

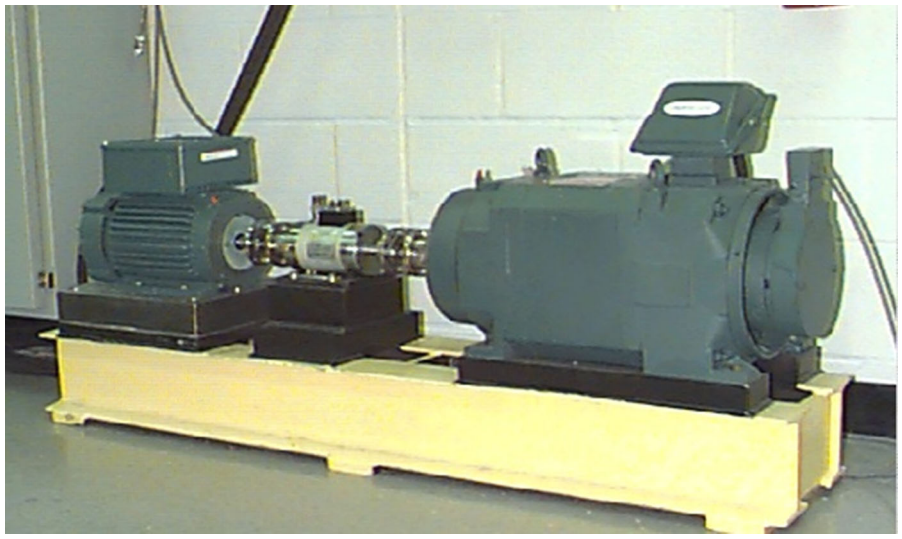

Fig. 14 A rolling-bearing experiment for modeling bearing faults

Table 1 Twelve types of rolling-bearing fault and their specifications

Bearing conditions	Abbreviations of bearing fault specifications	Fault diameter (inches)	Fault depth (inches)
Normal	Normal	–	–
Inner race faults	IR007	0.007	0.011
	IR014	0.014	0.011
	IR021	0.021	0.011
	IR028	0.028	0.050
Ball faults	B007	0.007	0.011
	B014	0.014	0.011
	B021	0.021	0.011
	B028	0.028	0.150
Outer race faults	OR007	0.007	0.011
	OR014	0.014	0.011
	OR021	0.021	0.011

paper was adopted to probe these bearing vibration signals, and the results are illustrated in Fig. 20. As illustrated in Fig. 20, these symbols can be almost divided into twelve groups: normal, IR007, IR014, IR021, IR028, B007, B014, B021, B028, OR007, OR014 and OR021. Hence, the proposed method in this paper has the capability to distinguish between these twelve types of bearing condition.

4.3 Discussions

This paper compares the performance of skewness, kurtosis, PeEn, MPeEn and the proposed method in this paper numerically and experimentally. Consequently, skewness and kurtosis are not entirely reliable for describing machinery conditions. Moreover, PeEn frequently undergoes a small change over time for a single machinery condition. This means that PeEn may not be highly reliable for characterizing machinery conditions. In addition, MPeEn illustrates a considerable change over time for a single machinery condition due to an average procedure. This means that MPeEn may lack reliability for characterizing machinery conditions. Also, the proposed method in this paper performs well in describing machinery conditions both numerically and experimentally.

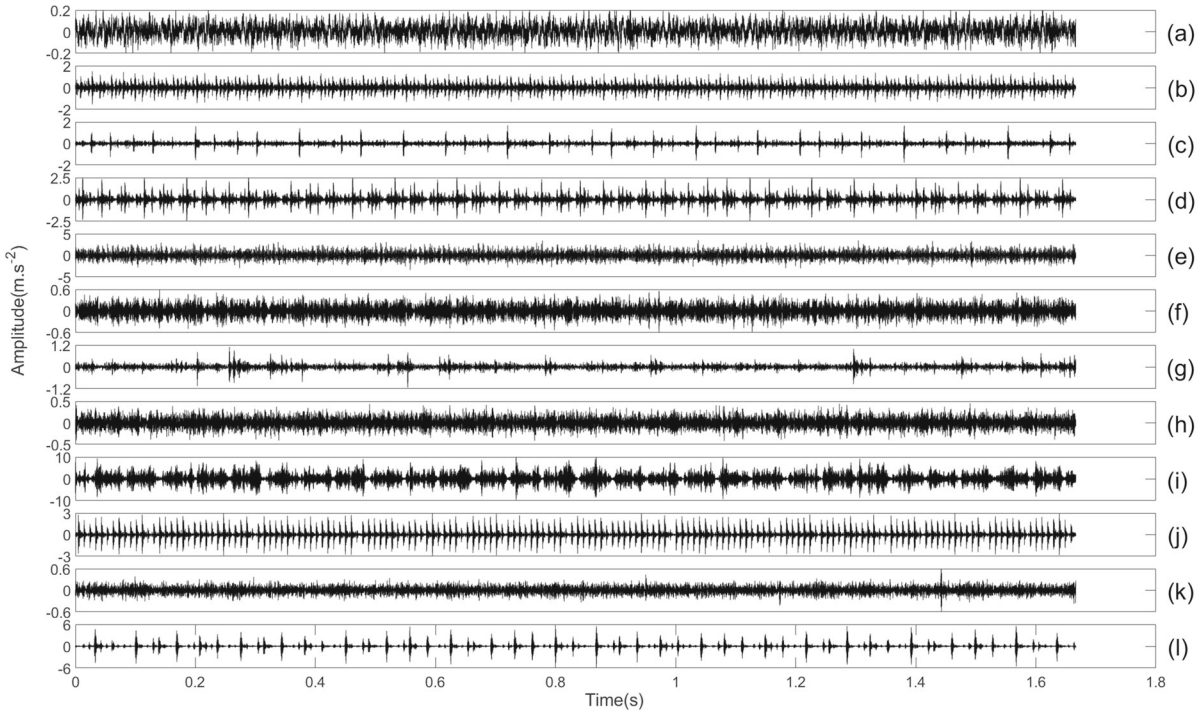

Fig. 15 Twelve types of bearing vibration signal in the rolling-bearing experiment, (a)–(l) for normal, IR007, IR014, IR021, IR028, B007, B014, B021, B028, OR007, OR014 and OR021, respectively

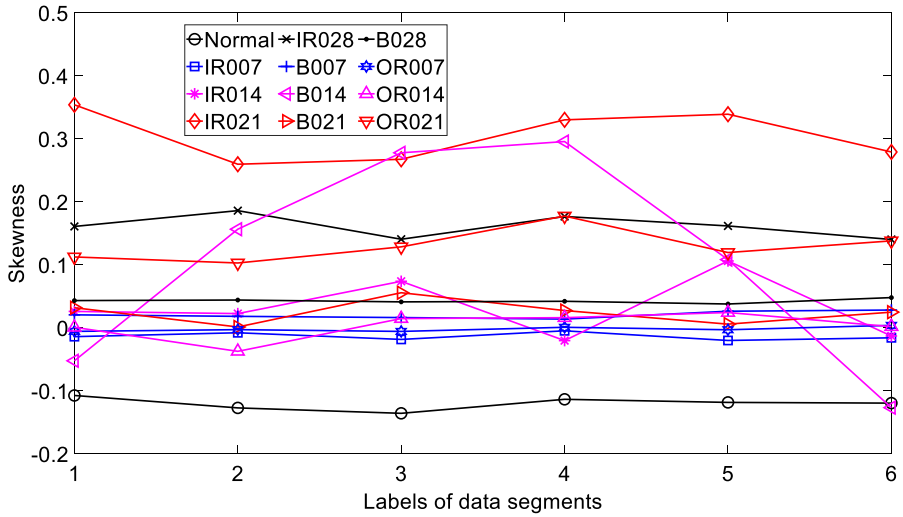

Fig. 16 Skewness for twelve types of bearing vibration signal

Thus, these comparisons show that the proposed method in this paper has a clear advantage over skewness, kurtosis, PeEn and MPeEn in describing machinery conditions. Additionally, the proposed method in this paper delivers an excellent performance in distinguishing between different types and severity of machinery faults.

This paper makes two main contributions. First, this paper generalizes PeEn to GPeEn by introducing different orders and time lags into PeEn. Indeed, orders and time lags make a considerable impact on PeEn, as demonstrated in this paper. Accordingly, it is really necessary to consider orders and time lags for PeEn. As a consequence, GPeEn can more fully reflect

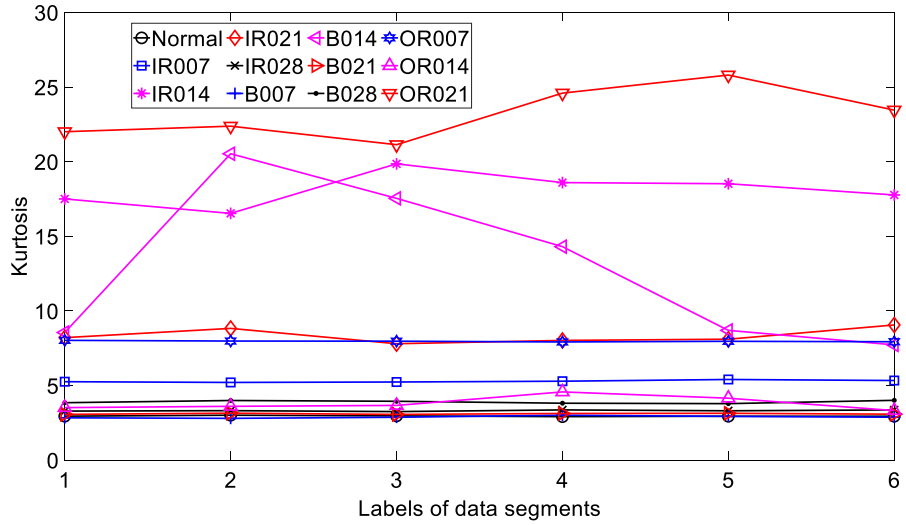

Fig. 17 Kurtosis for twelve types of bearing vibration signal

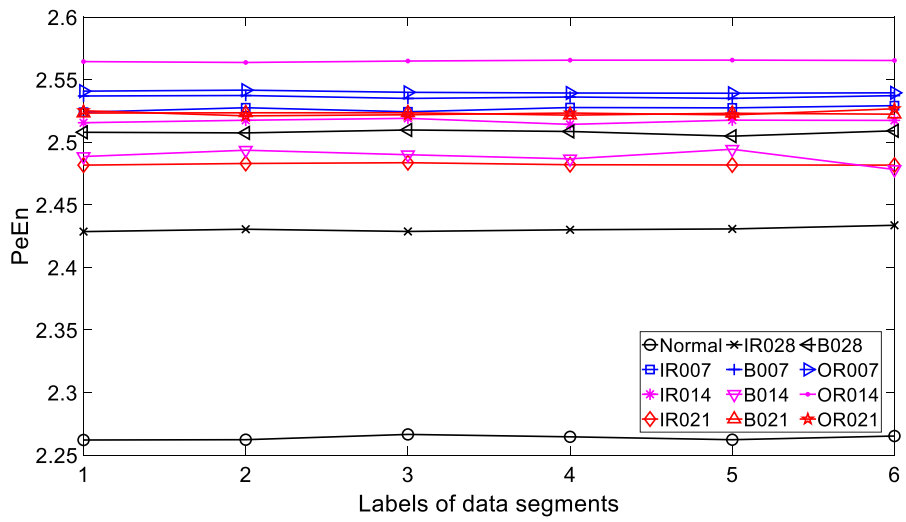

Fig. 18 PeEn for twelve types of bearing vibration signal

nature of machinery vibration signals than PeEn. Second, minimal, maximal and average values of the PeEn matrix obtained by GPeEn are exploited to describe machinery conditions. Consequently, this enables application of GPeEn in describing machinery conditions. Both numerical and experimental examples prove that the proposed method in this paper can effectively characterize conditions of a complex dynamic system.

Although performing well in characterizing conditions of complex dynamic systems, the proposed method in this paper still runs into some difficulties. For one thing, GPeEn has a higher time cost than PeEn and MPeEn. Currently, GPeEn seems slightly difficult for online application. For another, although the minimum, the maximum and the average values of a PeEn matrix can be always extracted, properties of a PeEn matrix need investigating further. Owing to a limit of spaces, these problems will be solved in the further.

5 Conclusions

This paper proposes GPeEn by introducing different orders and time lags into PeEn for relieving deficiencies of PeEn and MPeEn. Moreover, minimal, maximal and average values of a PeEn matrix obtained by GPeEn serve to briefly describe conditions of rotating machinery. Afterward, a simulation proves that the

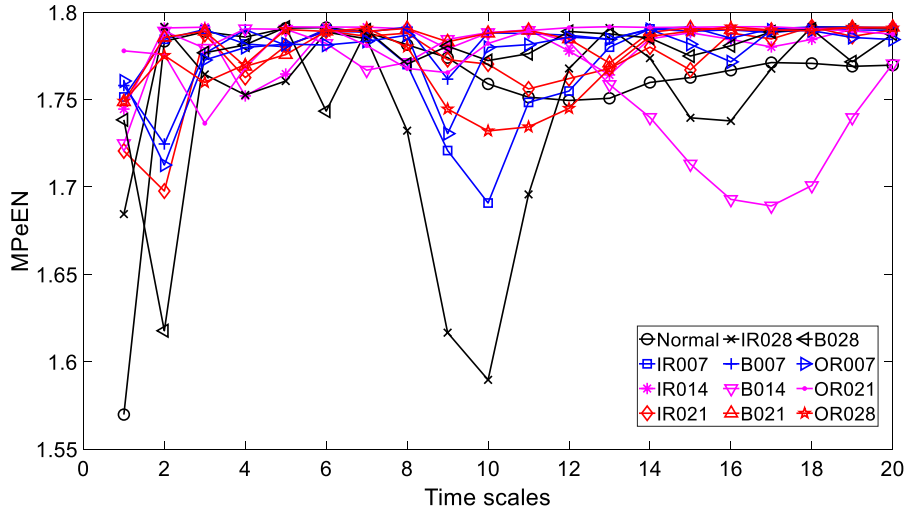

Fig. 19 MPeEn for twelve types of bearing vibration signal

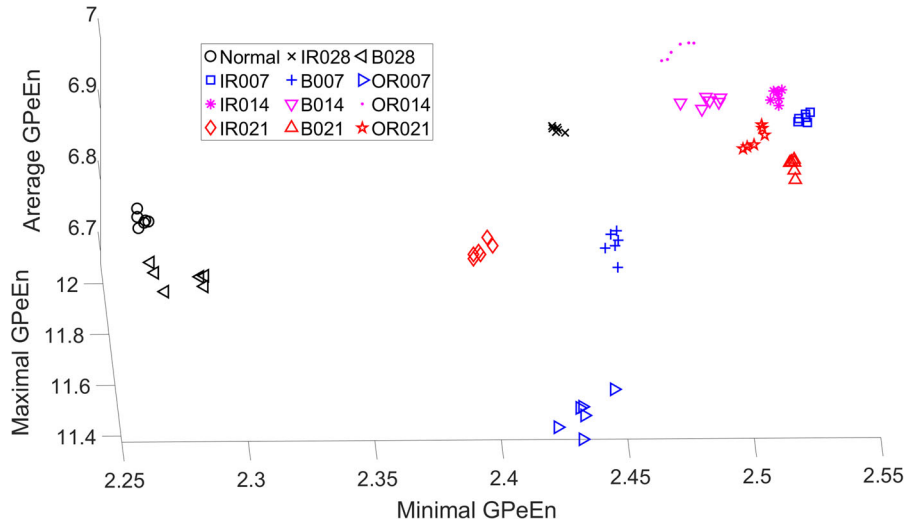

Fig. 20 Separation of twelve types of bearing condition by the proposed method in this paper

proposed method in this paper performs better than skewness, kurtosis, PeEn and MPeEn in describing conditions of a Lorenz model. Afterward, the performance of the proposed method in this paper was compared with that of skewness, kurtosis, PeEn and MPeEn by examining machinery vibration signals containing different types and severity of machinery faults. The results indicate that the proposed method in this paper delivers a better performance than skewness, kurtosis, PeEn and MPeEn in describing machinery conditions. This paper seems to develop a powerful method for condition monitoring of rotating machinery.

Acknowledgements Authors would like to kindly thank Bearing Data Center of Case Western Reserve University for sharing rolling-bearing fault data. The work was supported by Shandong Provincial Natural Science Foundation China (ZR2012EEL07).

Data availability The datasets generated during and/or analyzed during the current study are available from the corresponding author on reasonable request.

Declarations

Conflict of interest The authors declare that they have no conflict of interest.

References

1. Lin, J., Dou, C., Liu, Y.: Multifractal detrended fluctuation analysis based on optimized empirical mode decomposition for complex signal analysis. Nonlinear Dyn. **103**(3), 2461–2474 (2021). https://doi.org/10.1007/s11071-021-06223-7
2. Liu, Z., Zhang, L.: A review of failure modes, condition monitoring and fault diagnosis methods for large-scale wind turbine bearings. Measurement **149**, 107002 (2020). https://doi.org/10.1016/j.measurement.2019.107002
3. Wang, T., Han, Q., Chu, F., Feng, Z.: Vibration based condition monitoring and fault diagnosis of wind turbine planetary gearbox: a review. Mech. Syst. Signal Process. **126**, 662–685 (2019). https://doi.org/10.1016/j.ymssp.2019.02.051
4. Rajasekhar, M., Srinivas, J., Divekar, A.: Dynamic analysis of aero-engine rotors supported on ball bearing system. In: Proceedings of 1st International and 16th National Conference on Machines and Mechanisms (iNaCoMM2013), pp. 941–946 (2013)
5. Yang, J., Huang, D., Zhou, D., Liu, H.: Optimal IMF selection and unknown fault feature extraction for rolling bearings with different defect modes. Measurement **157**, 107660 (2020). https://doi.org/10.1016/j.measurement.2020.107660
6. Liang, P., Deng, C., Wu, J., Yang, Z.: Intelligent fault diagnosis of rotating machinery via wavelet transform, generative adversarial nets and convolutional neural network. Measurement **159**, 107768 (2020). https://doi.org/10.1016/j.measurement.2020.107768
7. Zair, M., Rahmoune, C., Benazzouz, D.: Multi-fault diagnosis of rolling bearing using fuzzy entropy of empirical mode decomposition, principal component analysis, and SOM neural network. Proc. Inst. Mech. Eng. Part C **233**(9), 3317–3328 (2019). https://doi.org/10.1177/0954406218805510
8. Chen, B., Shen, B., Chen, F., Tian, H., Xiao, W., Zhang, F., Zhao, C.: Fault diagnosis method based on integration of RSSD and wavelet transform to rolling bearing. Measurement **131**, 400–411 (2019). https://doi.org/10.1016/j.measurement.2018.07.043
9. Cheng, Y., Wang, Z., Chen, B., Zhang, W., Huang, G.: An improved complementary ensemble empirical mode decomposition with adaptive noise and its application to rolling element bearing fault diagnosis. ISA Trans. **91**, 218–234 (2019). https://doi.org/10.1016/j.isatra.2019.01.038
10. Huang, N.E., Shen, Z., Long, S.R., Wu, M.C., Shih, H.H., Zheng, Q., Yen, N.-C., Tung, C.C., Liu, H.H.: The empirical mode decomposition and the Hilbert spectrum for nonlinear and non-stationary time series analysis. Proc. R. Soc. Lond. A Math. Phys. Eng. Sci. **454**(1971), 903–995 (1998). https://doi.org/10.1098/rspa.1998.0193
11. Wu, Z., Huang, N.E.: Ensemble empirical mode decomposition: a noise-assisted data analysis method. Adv. Adapt. Data Anal. **1**(1), 1–41 (2009). https://doi.org/10.1142/S1793536909000047
12. Smith, J.S.: The local mean decomposition and its application to EEG perception data. J. R. Soc. Interface **2**(5), 443–454 (2005). https://doi.org/10.1098/rsif.2005.0058
13. Frei, M.G., Osorio, I.: Intrinsic time-scale decomposition: time-frequency-energy analysis and real-time filtering of non-stationary signals. Proc. R. Soc. A **463**(2078), 321–342 (2007). https://doi.org/10.1098/rspa.2006.1761
14. Medina, R., Macancela, J.-C., Lucero, P., Cabrera, D., Cerrada, M., Sánchez, R.-V., Vásquez, R.E.: Vibration signal analysis using symbolic dynamics for gearbox fault diagnosis. Int. J. Adv. Manuf. Technol. **104**(5), 2195–2214 (2019). https://doi.org/10.1007/s00170-019-03858-0
15. Lin, J., Chen, Q.: A novel method for feature extraction using crossover characteristics of nonlinear data and its application to fault diagnosis of rotary machinery. Mech. Syst. Signal Process. **48**(1), 174–187 (2014). https://doi.org/10.1016/j.ymssp.2014.04.007
16. Lin, J., Dou, C.: A novel method for condition monitoring of rotating machinery based on statistical linguistic analysis and weighted similarity measures. J. Sound Vib. **390**, 272–288 (2017). https://doi.org/10.1016/j.jsv.2016.12.005
17. Lin, J., Chen, Q.: Fault diagnosis of rolling bearings based on multifractal detrended fluctuation analysis and mahalanobis distance criterion. Mech. Syst. Signal Process. **38**(2), 515–533 (2013). https://doi.org/10.1016/j.ymssp.2012.12.014
18. Du, W., Kang, M., Pecht, M.: Fault diagnosis using adaptive multifractal detrended fluctuation analysis. IEEE Trans. Ind. Electron. **67**(3), 2272–2282 (2019). https://doi.org/10.1109/TIE.2019.2892667
19. Gao, Z., Jin, N.: Complex network from time series based on phase space reconstruction. Chaos **19**(3), 033137 (2009). https://doi.org/10.1063/1.3227736
20. Peng, Y., Xiang, W.: Short-term traffic volume prediction using GA-BP based on wavelet denoising and phase space reconstruction. Physica A **549**, 123913 (2020). https://doi.org/10.1016/j.physa.2019.123913
21. Kennel, M.B., Brown, R., Abarbanel, H.D.: Determining embedding dimension for phase-space reconstruction using a geometrical construction. Phys. Rev. A **45**(6), 3403 (1992). https://doi.org/10.1103/PhysRevA.45.3403
22. Zhang, S., Yang, J., Zhang, J., Liu, H., Hu, E.: On bearing fault diagnosis by nonlinear system resonance. Nonlinear Dyn. **98**(3), 2035–2052 (2019). https://doi.org/10.1007/s11071-019-05305-x
23. Hao, B.L.: Symbolic dynamics and characterization of complexity. Physica D **51**(1–3), 161–176 (1991). https://doi.org/10.1016/0167-2789(91)90229-3
24. Bandt, C., Pompe, B.: Permutation entropy: a natural complexity measure for time series. Phys. Rev. Lett. **88**(17), 174102 (2002). https://doi.org/10.1103/PhysRevLett.88.174102
25. Yan, R., Liu, Y., Gao, R.X.: Permutation entropy: a nonlinear statistical measure for status characterization of rotary machines. Mech. Syst. Signal Process. **29**, 474–484 (2012). https://doi.org/10.1016/j.ymssp.2011.11.022
26. Zheng, J., Dong, Z., Pan, H., Ni, Q., Liu, T., Zhang, J.: Composite multi-scale weighted permutation entropy and extreme learning machine based intelligent fault diagnosis for rolling bearing. Measurement **143**, 69–80 (2019). https://doi.org/10.1016/j.measurement.2019.05.002

27. Tian, Z., Li, S., Wang, Y.: A prediction approach using ensemble empirical mode decomposition-permutation entropy and regularized extreme learning machine for short-term wind speed. Wind Energy **23**(2), 177–206 (2020). https://doi.org/10.1002/we.2422
28. Landauskas, M., Cao, M., Ragulskis, M.: Permutation entropy-based 2D feature extraction for bearing fault diagnosis. Nonlinear Dyn. **102**(3), 1717–1731 (2020). https://doi.org/10.1007/s11071-020-06014-6
29. Tao, M., Poskuviene, K., Alkayem, N.F., Cao, M., Ragulskis, M.: Permutation entropy based on non-uniform embedding. Entropy **20**(8), 612 (2018)
30. Zunino, L., Olivares, F., Scholkmann, F., Rosso, O.A.: Permutation entropy based time series analysis: Equalities in the input signal can lead to false conclusions. Phys. Lett. A **381**(22), 1883–1892 (2017)
31. Amigó, J.M., Dale, R., Tempesta, P.: A generalized permutation entropy for noisy dynamics and random processes. Chaos **31**(1), 013115 (2021)
32. Aziz, W., Arif, M.: Multiscale permutation entropy of physiological time series. In: Pakistan Section Multitopic Conference, Karachi, Pakistan, 24–25 Dec., pp. 1–6. IEEE (2005)
33. Li, Y., Xu, M., Wei, Y., Huang, W.: A new rolling bearing fault diagnosis method based on multiscale permutation entropy and improved support vector machine based binary tree. Measurement **77**, 80–94 (2016)
34. Parlitz, U., Berg, S., Luther, S., Schirdewan, A., Kurths, J., Wessel, N.: Classifying cardiac biosignals using ordinal pattern statistics and symbolic dynamics. Comput. Biol. Med. **42**(3), 319–327 (2012). https://doi.org/10.1016/j.compbiomed.2011.03.017
35. Bandt, C.: Ordinal time series analysis. Ecol. Model. **182**(3–4), 229–238 (2005)
36. Cao, Y., Tung, W.-W., Gao, J., Protopopescu, V.A., Hively, L.M.: Detecting dynamical changes in time series using the permutation entropy. Phys. Rev. E **70**(4), 046217 (2004)
37. Takens, F.: Detecting strange attractors in turbulence. In: Dynamical Systems and Turbulence, Warwick 1980, pp. 366–381. Springer (1981)
38. Liu, B., Peng, J.: Nonlinear Dynamics. Higher Education Press, Beijing (2004)